Free Radical Research, June 2010; 44(6): 679–693

HOX-1 and COX-2: Two differentially regulated key mediators of skeletal myoblast tolerance under oxidative stress

IOANNA-KATERINA AGGELI, EIRINI KEFALOYIANNI, ISIDOROS BEIS & CATHERINE GAITANAKI

Department of Animal and Human Physiology, School of Biology, Faculty of Sciences, University of Athens, Panepistimioupolis, Athens 157 84, Greece

(Received date: 11 January 2010; In revised form date: 16 February 2010)

Abstract

The exact physiological role of oxidative stress as a primary cause for skeletal muscle pathological conditions involving muscle degeneration remains elusive. Therefore, the present study was performed so as to decipher the signalling pathways orchestrating the potential cytoprotective role of heme oxygenase 1 (HOX-1) as well as cyclooxygenase 2 (COX-2) in skeletal myoblasts exposed to H_2O_2. Cell treatment with H_2O_2 (0.5 mM) resulted in a time- and dose-dependent response of HOX-1 and COX-2 mRNA and protein levels, with ERK1/2, p38-MAPK and MSK1 found to mediate these effects. Furthermore, Src and JNKs blockade attenuated COX-2 response. Collectively, these novel findings highlight for the first time HOX-1 and COX-2 fundamental contribution to skeletal myoblast tolerance under oxidative stress, since their inhibition significantly attenuated viability of skeletal myoblasts. The data also delineate the various effectors regulating HOX-1 and COX-2 expression, probably alleviating muscle degeneration in related disorders.

Keywords: *HOX-1, COX-2, protein kinases, survival, skeletal myoblast, hydrogen peroxide*

Abbreviations: *AP1, Activator protein 1; BSA, Bovine serum albumin; COX-2, Cyclooxygenase 2; DMSO, Dimethylsulphoxide; EMSA, Electrophoretic mobility shift assay; ERK1/2, Extracellular signal-regulated kinases; GAPDH, Glyceraldehyde-3-phosphate dehydrogenase; HOX-1, Heme oxygenase 1; JNKs, cJun-N-terminal kinases; MAPKs, Mitogen-activated protein kinases; MSK1, Mitogen and stress activated kinase; PCR, polymerase chain reaction;* PGE_2*, Prostaglandin E2; SDS-PAGE, Sodium dodecyl sulphate-polyacrylamide gel electrophoresis; ZnPP, zinc protoporphyrin*

Introduction

Stressful conditions trigger a complex network of compensatory cellular responses that ensure preservation of cell homeostasis or induce apoptosis. Reactive oxygen species (ROS) have been found to act as signalling molecules modulating diverse biological processes exerting either beneficial or detrimental effects [1]. Thus, elevated levels of ROS may cause injury, resulting in severe pathological states including skeletal muscle disorders, i.e. sarcopenia, Duchenne and Becker muscular dystrophies [2,3]. Given that differentiated skeletal muscle cells have lost the ability to proliferate and that regeneration can mainly be achieved through myoblasts [4], it is of high importance to unravel the signal transduction pathways involved in their response to oxidative stress. The C2 cell line, which originated from crush injured mouse muscular myogenic cells, constitutes a widely used model closely resembling satellite cells in adult skeletal muscle [5]. Therefore, these cells comprise an ideal experimental setting for studying and elucidating the biochemical cascades responsible for compensation of oxidative stress, ensuring skeletal muscle function.

Correspondence: Professor Catherine Gaitanaki, Department of Animal and Human Physiology, School of Biology, University of Athens, Panepistimioupolis, Ilissia, Athens 157 84, Greece. Tel: +30 (210)7274136. Fax: +30 (210)7274635. Email: cgaitan@biol.uoa.gr

ISSN 1071-5762 print/ISSN 1029-2470 online © 2010 Informa UK Ltd. (Informa Healthcare, Taylor & Francis AS)
DOI: 10.3109/10715761003742985

C2 skeletal myoblasts exquisite tolerance to high ROS levels, previously established by our group [6], comprises a unique feature of these cells compared to other cell types. Therefore, the denomination of the principal 'mediators' of this feature is intriguing. H_2O_2 being more stable than other ROS and diffusing freely through membranes [7], we made an effort to investigate the H_2O_2-triggered C2 skeletal myoblast responses and examine their respective regulatory signal transduction mechanisms.

Excessive levels of free radicals are counteracted via upregulation of endogenous enzymatic or non-enzymatic systems (i.e. thioredoxin, glutathione peroxidase, catalase) [8] as well as other redox-related proteins such as heme oxygenase 1 (HOX-1) [9]. HOX-1, in particular, exhibits its antioxidant activity by acting as the rate-limiting enzyme in heme catabolism, yielding biliverdin, carbon monoxide (CO) and free iron (Fe^{2+}) [10]. Interestingly, there is ample evidence demonstrating that HOX-1 is induced by a plethora of stimuli including heavy metals, UV radiation, heat shock, inflammatory cytokines, prostaglandins and oxidative stress [11,12] and exerts a cytoprotective role. Therefore, it appeared intriguing to probe into its potential role in the present study. Furthermore, an effort was undertaken in order to explore cyclooxygenase-2 (COX-2) possible involvement in the H_2O_2-triggered response in skeletal myoblasts, since H_2O_2 is known to stimulate prostaglandin (PG) production *in vivo* [13] and COX is responsible for the generation of PGH_2, the main precursor molecule of all prostanoids, including PGE_2 [14]. Among the isoforms of COX identified so far, COX-1 is constitutively expressed, while COX-2 has a more limited distribution pattern and is transiently induced by various stimuli including cytokines, mitogens, cell injury and hyperosmolarity [15,16]. Several studies have also implicated COX-2 in skeletal myoblasts stretch-induced proliferation [3], as well as in the early stages of skeletal muscle regeneration [17].

Various reports have focused on the intermediacy of mitogen-activated protein kinases (MAPKs) in both HOX-1 and COX-2 regulation, depending on the experimental model and the stimulus examined [18,19]. MAPKs consist of three major and extensively characterized sub-families: the extracellular signal-regulated kinases 1 and 2 (ERK1/2), c-Jun N-terminal kinases (JNKs) and p38-MAPK [20]. These Ser/Thr kinases can be activated by growth factors, mitogens and various types of environmental stress. Upon activation, MAPKs interact with their target-substrates that include other protein kinases (MAPKAPK2, MSK1), cytoskeletal proteins (i.e. tau) as well as transcription factors (Elk-1, ATF-2, c-Jun, NF-κB) located both in the cytoplasm and the nucleus [20]. The above-mentioned MAPK sub-families have all been shown to be activated by oxidative stress, leading to the stimulation of apoptotic or cell survival mechanisms depending on the type, strength and the duration of the stimulus, as well as the cell type studied [6,21]. Among the redox-sensitive transcription factors that modulate gene expression under oxidative stress conditions, a pivotal role has been attributed to nuclear factor κB (NF-κB) and activator protein 1 (AP1) [22]. What is more, the mitogen- and stress-activated kinase 1 (MSK1), another MAPKs substrate, has been shown to participate in the activation of these transcription factors via phosphorylation of the p65 sub-unit of NF-κB [23] and of AP1 components: cJun and ATF2 [18].

Overall, the present study was designed to address HOX-1 and COX-2 potential contribution to skeletal myoblast tolerance to oxidative stress as well as the signalling pathways involved in the regulation of their expression. Furthermore, our findings also offer for the first time a better understanding of COX-2 pro-survival role in oxidative stress-exposed skeletal myoblasts.

Materials and methods

Materials

All chemicals were of the highest grade available and purchased from Sigma-Aldrich Chemie GmbH (89552 Steinheim, Germany) and Merck (Darmstadt 64293, Germany). The enhanced chemiluminescence (ECL) kit was from Amersham International (Uppsala, Sweden). Bradford protein assay reagent was from Bio-Rad (Hercules, CA). Nitrocellulose (0.45 μm) was obtained from Schleicher & Schuell (Keene, NH). The selective inhibitors SB203580 (#559389), PD98059 (#513000), SP600125 (#4201119) and PP2 (#529573) were obtained from Calbiochem-Novabiochem (La Jolla, CA). The inhibitor H89 (#B1427) was from Sigma-Aldrich Chemie GmbH (Steinheim, Germany). COX-2 inhibitor: sc236 (#10004219) and PGE_2 immunoassay kit (#514010) were obtained from Cayman Chemical Company (Michigan). [γ^{32}P] ATP was from Hartmann Analytic GmbH (Braunschweig, Germany). The activator protein 1 (AP1) consensus oligonucleotide (#E3202), T4 polynucleotide kinase (M4101) and T4 polynucleotide kinase buffer (C1313) were obtained from Promega (Madison, WI). ZnPP (#282820) and poly dI-dC (P4929) were from Sigma-Aldrich Chemie GmbH. Antibodies specific for the phosphorylated forms of MSK1 (#9595), p65 NF-κB (#3037), c-Jun (#9261), ATF-2 (#9221) as well as antibodies specific for total c-Jun (#3037) and ATF-2 (#9222) were obtained from Cell Signaling Technology (Beverly, MA). The anti-actin was from Sigma-Aldrich (St. Louis, MO) while anti-histone-1 was from Neomarkers (Fremont, CA). Pre-stained molecular mass markers (#P7708) were from New England Biolabs (Beverly, MA). HRP-conjugated anti-rabbit (#P0448) and

anti-mouse (#P0447) antibodies were from DAKO A/S (DK-2600 Glostrup, Denmark). Fluorescent dye-labelled anti-rabbit IgG Alexa Fluor® 488 (#A-11008) and Alexa Fluor® 594 (#A-11012) were from Invitrogen-Molecular Probes (Eugene, OR). Super RX film (24 × 18 cm) was purchased from FujiFilm Europe GmbH (Dusseldorf, Germany). TRIzol® reagent (#15596-026) and Reverse Tanscriptase M-MLV (#28025-013) were obtained from Invitrogen Life Technologies (California). Taq polymerase (#101025) was from Bioron GmbH (Ludwigshafen, Germany). Cell culture reagents including foetal bovine serum (FBS #A15-043), Dulbecco's Modified Eagle's Medium (DMEM #E15-843), antibiotics (penicillin, streptomycin #P11-010) and Trypsin/EDTA were purchased from PAA Laboratories GmbH (Pasching, Austria). GelRed™ 10,000X solution in water (#41003) was obtained from Biotium Inc. (Hayward, CA).

Cell cultures and treatments

In all experiments, C2 murine myoblasts were used. This cell line was kindly provided by Dr Yaffe [5]. Cells were grown in a humidified 95% air–5% CO_2 atmosphere, in DMEM supplemented with 15% (v/v) heat inactivated foetal bovine serum (FBS), 100 U/ml penicillin and 100 µg/ml streptomycin. Experiments were carried out at a 70% confluence and after at least 3 h of serum deprivation. Exogenous H_2O_2 was used as the oxidant agent at the concentrations and for the times indicated. When pharmacological inhibitors were used they were dissolved in DMSO and added to the medium 30 min prior to treatment with H_2O_2, with the exception of sc236, which was dissolved in ethanol and was added to the medium 60 min prior to treatments. Control experiments with DMSO or ethanol alone were also performed for the same duration (data not shown).

Protein extraction

Cells were extracted in buffer G (20 mM Hepes, pH 7.5, 20 mM β-glycerophosphate, 20 mM NaF, 2 mM EDTA, 0.2 mM Na_3VO_4, 5 mM dithiothreitol (DTT), 10 mM benzamidine, 200 µM leupeptin, 10 µM trans-epoxy succinyl-L-leucylamido-(4-guanidino) butane, 300 µM phenyl methyl sulphonyl fluoride (PMSF), 0.5%(v/v) Triton X-100) and incubated on ice for 30 min. Samples were centrifuged (10 000 g, 5 min, 4°C) and the supernatants were boiled with 0.33 volumes of SDS/PAGE sample buffer (4X) (0.33 M Tris/HCl, pH 6.8, 10% (w/v) SDS, 13% (v/v) glycerol, 20% (v/v) 2-mercaptoethanol, 0.2% (w/v) bromophenol blue). Protein concentrations were determined using the BioRad Bradford assay.

Preparation of nuclear extracts

Cells were harvested in Buffer A (10 mM Hepes pH 7.9, 10 mM KCl, 0.1 mM EGTA, 0.1 mM EDTA, 1.5 mM $MgCl_2$, 10 mM NaF, 1 mM Na_3VO_4, 20 mM β-glycerophosphate, 2 µg/mL leupeptin, 1 mM DDT, 0.5 mM PMSF, 4 µg/mL aprotinin) and incubated on ice for 15 min. Samples were centrifuged (1400 *g*, 5 min, 4°C) and the supernatants discarded. Pellets were washed with Buffer A containing 0.1% (v/v) Nonidet P40 and centrifuged (1400 *g*, 5 min, 4°C). Subsequently, pellets were re-suspended in Buffer B (20 mM Hepes pH 7.9, 0.4 M NaCl, 1 mM EGTA, 0.1 mM EDTA, 1.5 mM $MgCl_2$, 10 mM NaF, 1 mM Na_3VO_4, 20 mM β-glycerophosphate, 2 µg/mL leupeptin, 0.2 mM DDT, 0.5 mM PMSF, 4 µg/mL aprotinin) and incubated under rotation, for 1 h at 4°C. After centrifugation (11 000 *g*, 10 min, 4°C), protein concentrations in the supernatants (containing the nuclear protein) were determined using the BioRad Bradford assay and samples were either stored at −80°C for use in the electrophoretic mobility shift assays (EMSAs) or boiled with 0.33 volumes of SDS/PAGE sample buffer (4X) for Western blot analysis.

Western blot

Proteins (20 µg) were separated by SDS-PAGE on 10% (w/v) acrylamide, 0.275% (w/v) bisacrylamide slab gels and transferred electrophoretically onto nitrocellulose membranes (0.45 µm). Membranes were then incubated in TBS-T (20 mM Tris-HCl, pH 7.5, 137 mM NaCl, 0.05% (v/v) Tween 20) containing 5% (w/v) non-fat milk powder for 30 min at room temperature (R_T). Subsequently, membranes were incubated overnight with the appropriate antibody, according to the manufacturer's instructions. After washing in TBS-T (3 × 10 min) blots were incubated with horse-radish peroxidase-linked anti-rabbit or anti-mouse IgG antibodies (1:5000 dilution in TBS-T containing 1% (w/v) non-fat milk powder, 1 h, R_T). After washing in TBS-T (3 × 10 min) bands were detected using enhanced chemiluminescence and quantified by scanning densitometry (Gel Analyser v.1.0)

Electrophoretic mobility shift assay (EMSA)

The assay was performed as previously described [18]. Briefly, after labelling of the oligonucleotide containing consensus AP1 sequence (3.5 pmol) with [γ-^{32}P] ATP, unincorporated [γ-^{32}P] ATP was removed using a Sephadex G50 column in TE buffer (10 mM Tris–HCl pH 8.0, 1 mM EDTA). Nuclear extracts (10 µg) were incubated (10 min, R_T) in binding buffer (50 mM Tris–HCl pH 7.5, 250 mM NaCl, 5 mM EDTA, 25% (v/v) glycerol, 1 mM DTT, 1 µg poly

dI–dC) in a final volume of 20 µl. Subsequently, 0.5 ng of radiolabelled oligonucleotide was added (20 min, R_T). DNA–protein complexes were resolved on a 5% (w/v) non-denaturing polyacrylamide gel (120 V, 1 h). Gels were dried and exposed to Super RX photo film for 24 h at −80°C using an intensifying screen. For competition experiments, unlabelled cAP1 oligonucleotide (4–40 ng) was added prior to the addition of radiolabelled cAP1 (data not shown).

RNA extraction, cDNA synthesis and ratiometric reverse transcription PCR (RT-PCR)

Expression of endogenous HOX-1 and COX-2 mRNA levels was determined by ratiometric reverse transcription of total RNA followed by PCR analysis, as previously described [18]. Briefly, total RNA was extracted from cells using Trizol (Invitrogen Life Technologies) and, after cDNA synthesis, reverse transcription was performed with M-MLV Reverse Transcriptase (Invitrogen Life Technologies), first strand buffer (Promega, Madison, WI), dithiothreitol (Promega) and deoxy-nucleotide triphosphates (dNTPs) (Promega). PCR for HOX-1 was performed using 1.5 Units Taq (Bioron GmbH, Ludwigshafen, Germany) with the following primers: HOX-1 forward: 5′- TTG TTC GTC TTG GGT CAG AT -3′ and HOX-1 reverse: 5′- CCT TCT GTG CAA TCT TCT TC -3′; glyceraldehyde-3-phosphate dehydrogenase (GAPDH) forward: 5′- ACC ACA GTC CAT GCC ATC AC -3′ and GAPDH reverse: 5′- TCC ACC ACC CTG TTG CTG TA -3′; COX-2 forward: 5′- CCT GCT GCC CGA CAC CTT CA -3′ and COX-2 reverse: 5′- CAG ATG AGA GAC TGA ATT GAG GCA G -3′ based on the sequence of mouse HOX-1 and COX-2 (Genbank accession no NM010442 and NM011198, respectively). After a 5 s denaturation at 94°C, PCR was carried out as follows: 94°C for 30 s, 58°C for 30 s and 72°C for 30 s (26 cycles) for HOX-1; 94°C for 30 s, 59°C for 30 s and 72°C for 30 s (27 cycles) for COX-2 and 94°C for 30 s, 59°C for 30 s and 72°C for 30 s (25 cycles) for GAPDH with a final extension done at 72°C for 4 min. (GAPDH Genbank accession no. X02231). cDNA samples derived from 'control' (non-treated) and treated cells were always amplified simultaneously. PCR products were separated on a 2% (w/v) agarose gel and subsequently incubated for 20 min with GelRed™, which is an ultra sensitive, extremely stable and environmentally safe fluorescent nucleic acid dye. After densitometric analysis of PCR product bands using an appropriate image analysis programme (Gel Analyser v. 1.0), values were normalized for the respective values of GAPDH. Estimation of fragment band size (HOX-1 259bp, COX-2 540bp, GAPDH 452bp) was performed by comparison with GeneRuler 100-bp DNA ladder (Fermentas Life Sciences Inc., Hanover, NH).

Immunofluorescence staining

Cells were grown on 10 mm diameter coverslips in plating medium and were treated after serum had been withdrawn for at least 3 h. After washing in cold PBS, cells were fixed in methanol (−20°C) for 10 min. Cells were then washed (2 × 5 min) with TBS-T and incubated with 5% (w/v) BSA in TBS-T for 45 min (R_T) and subsequently with the appropriate primary antibody solution overnight (4°C). After washing in TBS-T (2 × 15 min) coverslips were incubated in the dark with either Alexa Fluor 488-conjugated anti-rabbit secondary antibody (1:250) (green fluorescense) or with Alexa Fluor(R) 594 (1:250) (red fluorescence) for 1 h (R_T). Following mounting, slides were visualized under a laser scanning confocal Zeiss Axiovert BioRad Radience 2100 microscope.

Cell viability assay

Cell viability was estimated using the MTT assay [24]. Cells were seeded in 96-well culture plates and treated with the oxidant for 24 h after serum had been withdrawn for at least 3 h. Four hours prior to the end of treatment, 50 µg MTT (3-[4,5-dimethylthiazol-2-yl]-2,5-diphenyltetrazolium bromide) were added to each well. Subsequently, cells were lysed in 0.1 M HCl/isopropanol and optical density was measured in an ELISA microplate reader (DENLEY, West Sussex, UK) using a 540 nm filter.

Measurement of PGE_2 levels

Culture media were collected at the end of the interventions examined and prostaglandin E_2 (PGE_2) levels were measured with a commercial immunoassay kit according to the manufacturer's instructions (Cayman).

Statistical evaluations

Western blot, EMSA, RT-PCR and confocal images shown are representative of at least three independent experiments. All data are expressed as mean ± SE. Differences between two groups were evaluated by Student's *t*-test. Data from more than two groups were evaluated by one-way analysis of variance (ANOVA) followed by Tukey multiple comparison test (Graph Pad Prism Software, San Diego, CA). A value of at least $p < 0.05$ was considered to be statistically significant.

Results

H_2O_2 stimulates a time- and dose-dependent increase in HOX-1 and COX-2 mRNA and protein levels

Heme oxygenase 1 (HOX-1) and cyclooxygenase 2 (COX-2) have been previously reported to favour cell survival under adverse redox conditions [16,25]. Therefore, as the first step in the present study, we examined the effect of H_2O_2 on their time- and dose-dependent response pattern in C2 skeletal myoblasts. Based on our previous findings [6], the effect of 0.5 mM of H_2O_2 was investigated and found to significantly induce HOX-1 transcript levels after 2 h of treatment. The response was maximized after 4 h (4.91 ± 0.12-fold, relative to control), decreasing thereafter but remaining statistically significant even after 24 h (Figures 1A and B, top left panels). Increasing H_2O_2 concentrations were found to induce a concomitant increase in HOX-1 mRNA levels, as evidenced in Figures 1A and B, top right panels. As an internal control, the mRNA levels of GAPDH were also examined in identical samples and found to remain constant (Figure 1, bottom panels). HOX-1 protein levels were observed to be maximally induced after 6 h of treatment with 0.5 mM H_2O_2 (3.75 ± 0.25-fold, relative to control) and remained statistically significant compared to control even after 24 h (Figures 2A and B, top left panels). Coinciding with the RT-PCR results, increasing H_2O_2 concentrations resulted in respectively upregulated HOX-1 protein levels, as shown in Figures 2A and B, top right panels. Equal protein loading was verified by reprobing the membranes with an anti-actin antibody (Figure 2, bottom panels).

As far as COX-2 response pattern is concerned, COX-2 transcript levels were found to be markedly induced by 0.5 mM of H_2O_2 after 2 h of treatment, attaining maximal values after 4 h (2.84 ± 0.22-fold, relative to control), decreasing thereafter (Figures 1A and B, middle left), while high concentrations of the oxidant led to a sustained increase of COX-2 mRNA levels (Figures 1A and B, middle right panels). COX-2 protein levels also exhibited a time- and dose-dependent profile after treatment with H_2O_2. In particular,

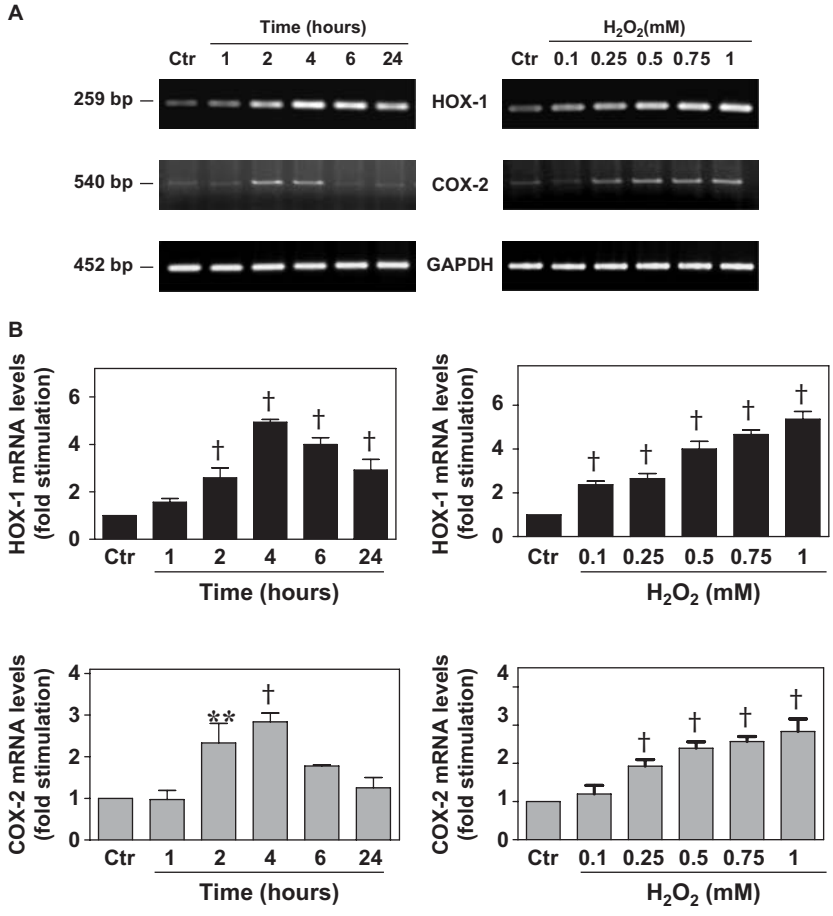

Figure 1. Time- and dose-dependent profile of HOX-1 and COX-2 mRNA up-regulation by H_2O_2. C2 skeletal myoblasts were left untreated (Ctr) or treated with 0.5 mM H_2O_2 for the times indicated (A, left panels) or with increasing concentrations of H_2O_2 for 4 h (A, right panels). Expression of HOX-1 (A, top panels), COX-2 (A, middle panels) as well as GAPDH (A, bottom panels) mRNA was analysed by ratiometric RT-PCR. PCR products band size is indicated on the left of the panels. After densitometric analysis of the PCR products, results were normalized for GAPDH and the data is presented as fold stimulation (B). Results are means ± SE for at least three independent experiments. $^{**}p < 0.05$, $^{\dagger}p < 0.001$ compared to control values (one-way ANOVA with Tukey post-test).

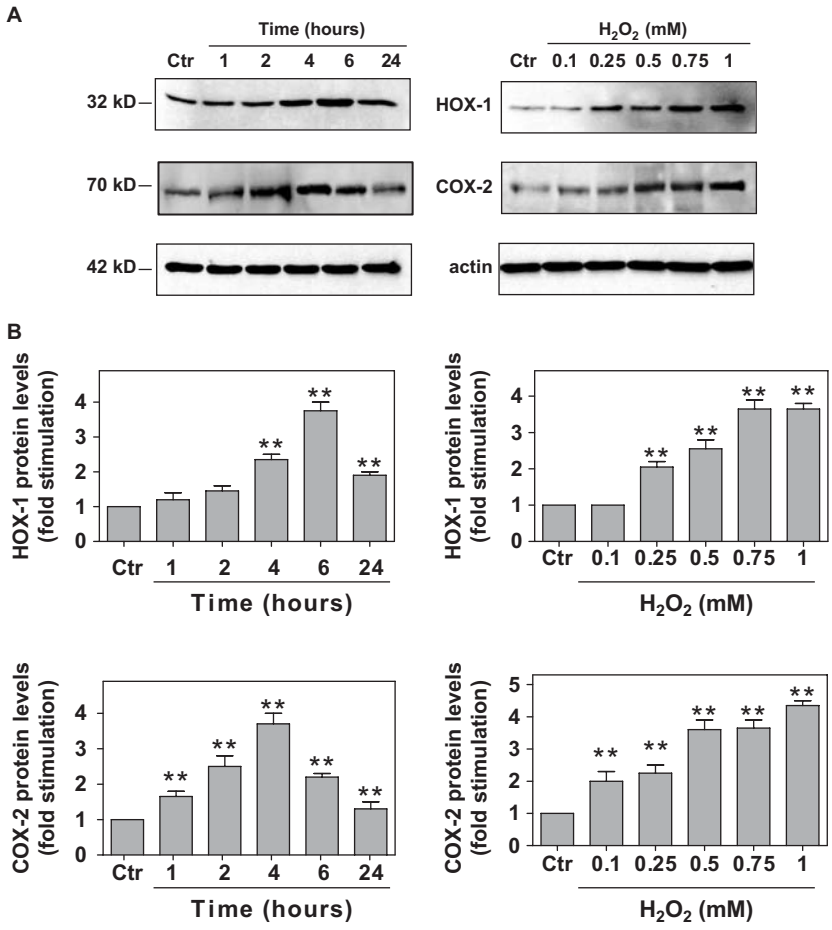

Figure 2. Time- and dose-dependent profile of HOX-1 and COX-2 protein up-regulation by H_2O_2. C2 skeletal myoblasts were left untreated (Ctr) or treated with 0.5 mM H_2O_2 for the times indicated (A, left panels) or with increasing concentrations of H_2O_2 for 4 h (A, right panels). Whole cell extracts (20 μg) were subjected to SDS-PAGE and immunoblotted with antibodies for total HOX-1 (A, top panels), COX-2 (A, middle panels) and actin (A, bottom panels) levels. Respective protein band size is indicated on the left of the panels. Bands were quantified by laser scanning densitometry (B). Blots and results shown are representative of at least three independent experiments. Results are means ± SE for at least three independent experiments. $^{**}p < 0.01$ compared to control values (one-way ANOVA with Tukey post-test).

maximal COX-2 protein levels were attained after 4 h (0.5 mM H_2O_2) by 3.71 ± 0.31-fold, relative to control (Figures 2A and B, middle left panels). Furthermore, increasing H_2O_2 concentrations were shown to significantly upregulate COX-2 protein levels (Figures 2A and B, middle right panels).

Diverse signalling pathways mediate HOX-1 and COX-2 expression by H_2O_2

In an attempt to decipher the signalling pathways involved in the regulation of the above responses, multiple selective pharmacological inhibitors were used. As shown in Figures 3A (top panel) and B: SB203580, PD98059 as well as H89 all partially attenuated H_2O_2-induced HOX-1 mRNA levels. This finding indicates that oxidative stress induces an up-regulation of HOX-1 transcripts via a mechanism involving p38-MAPK, MEK1/2 and MSK1, respectively. Similar results were observed while examining these inhibitors effect on H_2O_2-induced HOX-1 protein levels (Figures 3C and D). The inhibitors alone were confirmed to have no significant effect on HOX-1 mRNA or protein (Figures 3A and C). No inhibitory effect on H_2O_2-induced HOX-1 transcription or protein expression was observed when SP600125 (JNKs inhibitor) or PP2 (non-receptor Src tyrosine kinase inhibitor) were tested (data not shown).

On the contrary, our experiments using selective inhibitors revealed that ERK1/2, p38-MAPK and MSK1 along with JNKs and the non-receptor Src tyrosine kinase pathways are involved in H_2O_2-induced up-regulation of COX-2 mRNA and protein levels (Figure 4). DMSO or the inhibitors alone did not exhibit any significant effect on COX-2 mRNA or protein levels (data not shown).

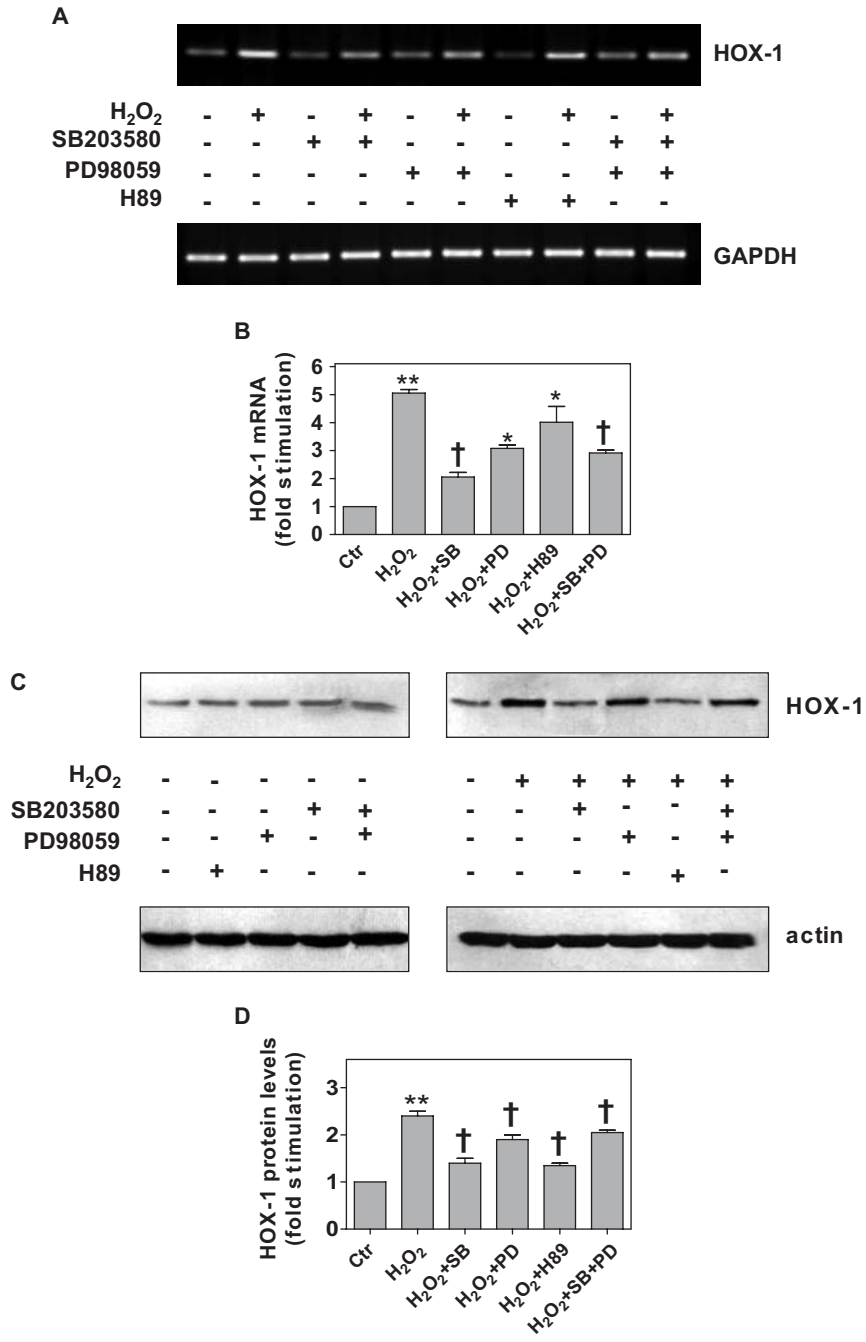

Figure 3. HOX-1 up-regulation by H_2O_2 is ERK1/2, p38-MAPK and MSK1-dependent. Cells were left untreated (Ctr) or pre-incubated with 10 μM SB203580 (+SB), 25 μM PD98059 (+PD) and 10 μM H89 (+H89) for 30 min and subsequently exposed to 0.5 mM H_2O_2 for 4 h. (A) Expression of HOX-1 (top panel) and GAPDH (bottom panel) mRNA was analysed by ratiometric RT-PCR and after densitometric analysis the data is presented as fold stimulation (B). (C) Whole cell extracts (20 μg) were subjected to SDS-PAGE and immunoblotted with antibodies for total HOX-1 (top panels) and actin (bottom panels) levels. Bands were quantified by laser scanning densitometry (D). The effect of the inhibitors alone is also shown. Results are means ± SE for at least three independent experiments. $^{**}p < 0.01$ compared to control values (one-way ANOVA with Tukey post-test) and $^{*}p < 0.05$, $^{\dagger}p < 0.001$ compared to identically treated cells in the absence of the respective inhibitor (two-tailed Student's *t*-test).

ERK1/2 and p38-MAPK are involved in H_2O_2-induced phosphorylation of MSK1 which is located in the nucleus, mediating NF-κB phosphorylation

Given the observed involvement of certain kinases in the regulation of both HOX-1 and COX-2 expression under oxidative stress conditions, an effort was next made to decipher the sub-cellular localization of the mediators transducing the oxidative signal in this particular experimental setting. Our results revealed H_2O_2-induced phospho-MSK1 immunoreactivity to be located exclusively in the nucleus (Figure 5A, H_2O_2), being diminished in the simultaneous presence

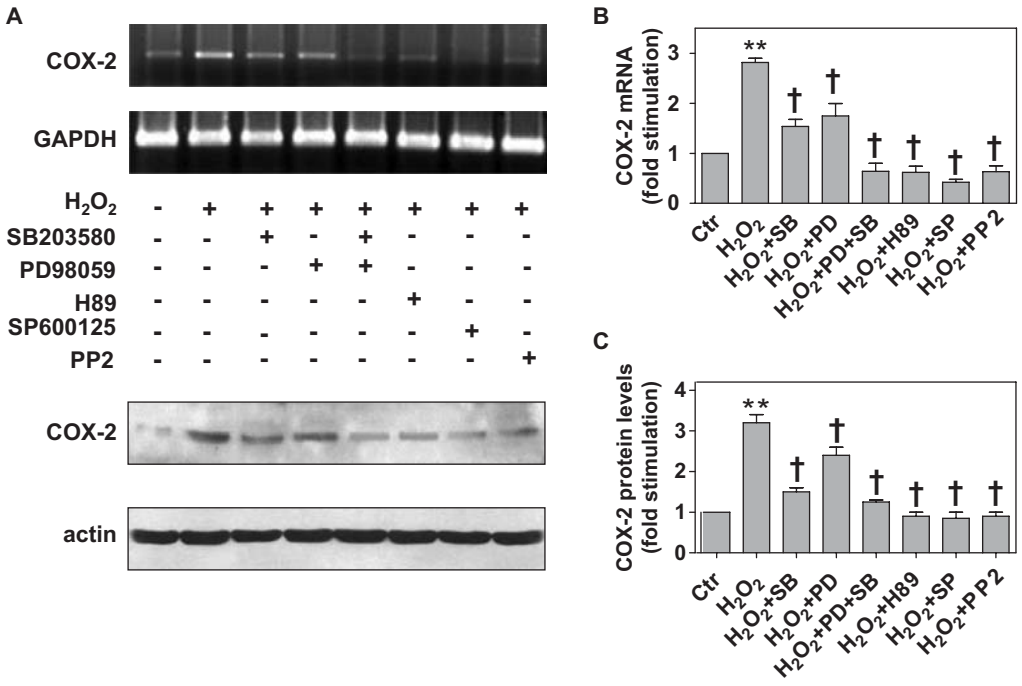

Figure 4. Multiple pathways are involved in COX-2 induction by H_2O_2. Cells were left untreated (Ctr) or pre-incubated with 10 μM SB203580 (+SB), 25 μM PD98059 (+PD), 10 μM H89 (+H89), 10 μM SP600125 or 10 μM PP2 for 30 min and then exposed to 0.5 mM H_2O_2 for 4 h. (A) Expression of COX-2 (1st panel) and GAPDH (2nd panel) mRNA was analysed by ratiometric RT-PCR. After densitometric analysis the data is presented as fold stimulation (B). (A) Whole cell extracts (20 μg) were subjected to SDS-PAGE and immunoblotted with antibodies for total COX-2 (3rd panel) and actin (4th panel) levels. Bands were quantified by laser scanning densitometry (C). Results are means ± SE for at least three independent experiments. $^{**}p < 0.01$ compared to control values (one-way ANOVA with Tukey post-test) and $^{\dagger}p < 0.001$ compared to identically treated cells in the absence of the respective inhibitor (two-tailed Student's *t*-test).

of PD98059 and SB203580. This result confirms MEK1/2 and p38-MAPK to be involved in MSK1 H_2O_2-induced phosphorylation (Figure 5A, H_2O_2 + PD + SB).

MSK1 has been previously established to mediate phosphorylation of the p65 sub-unit of NF-κB at Ser276 [6,23] and NF-κB has been shown to be transactivated under oxidative stress in this experimental model [6]. Thus, we set out to verify the subcellular localization of the latter. Our results clearly showed that H_2O_2-treatment enhanced the nuclear localization of phosphorylated p65 (Ser276) (Figure 5B, H_2O_2). Combined pre-treatment of cells with PD98059 and SB203580 (Figure 5B, H_2O_2 + PD + SB) as well as with the MSK1 selective inhibitor H89 (Figure 5B, H_2O_2 + H89), considerably attenuated this effect. This finding is indicative of ERK1/2 and p38-MAPK pathways participation in H_2O_2-induced phosphorylation of p65 at Ser276, possibly via the downstream mediation of MSK1.

H_2O_2 stimulates c-Jun and ATF2 phosphorylation as well as AP1 binding activity

With c-Jun and ATF2 constituting well established downstream MAPKs substrates and AP1 components [26–28], an effort was subsequently made to examine the time profile of their phosphorylation (hence activation), under the conditions investigated, in nuclear extracts. Both, c-Jun (at Ser63) and ATF2 (at Thr71) exhibited a similar time-dependent phosphorylation profile with maximal increase of their phosphorylation levels detected after treatment with H_2O_2 for 30 min (5.95 ± 0.34 and 3.65 ± 0.40-fold, relative to control, respectively) as shown in Figures 6A and B, top panels and respective graphs. Neither phosphorylated c-Jun nor phospho-ATF2 were detected in the respective cytoplasmic fractions (data not shown). Total c-Jun (Figure 6A, bottom panel) and ATF2 (Figure 6B, middle panel) levels were also detected in the respective samples without exhibiting any significant fluctuations. The presence of histone 1 immunoreactivity was detected in the nuclear extracts (Figure 6B, bottom panel).

We next probed into AP1 potential role in the response of skeletal myoblasts to H_2O_2 treatment. To this end, we monitored AP1 time- and dose-dependent DNA binding activity using EMSA. H_2O_2 (0.5 mM) was found to induce a relatively rapid increase in AP1 binding activity with maximal values attained within 30 min (7.768 ± 0.633-fold, relative to control) and maintained over 2 h of treatment (Figure 7A, top and bottom panels). Regarding the dose profile of H_2O_2-induced AP1 DNA binding activity,

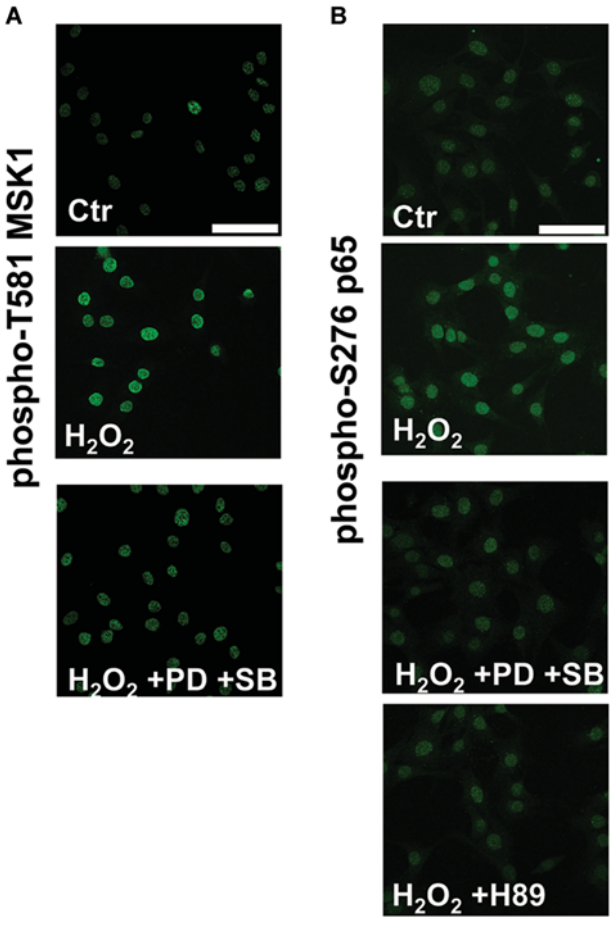

Figure 5. Distribution profile of phosphorylated MSK1 and NF-κB p65 sub-unit in C2 skeletal myoblasts left untreated (Ctr) or exposed to 0.5 mM H_2O_2 for 30 min (H_2O_2). Cells were subjected to immunocytochemical analysis with specific antibodies directed against phosphorylated MSK1 (A), NF-κB p65 sub-unit (B) (green fluorescence). Representative images are shown, indicative of at least three independent experiments. As indicated, myoblasts were pre-treated with PD98069 (+PD), SB203580 (+SB) or H89 (+H89) and subsequently exposed to H_2O_2. Slides were visualized by confocal microscopy. Scale bar: 80 μm.

maximal values were observed at 0.5–0.75 mM of the oxidant (Figure 7B, top and bottom panels). In the presence of 10-fold excess of non-radiolabelled AP-1 oligonucleotide, the detected H_2O_2-induced band of the autoradiograph was diminished (data not shown) confirming that it represents an AP-1 binding complex.

Further experiments revealed that selective inhibitors of JNKs (SP600125) and Src kinase (PP2) abolished the H_2O_2-induced up-regulation of AP1 DNA binding activity (Figure 7C, top and bottom panels). This finding indicates that JNKs and Src play a fundamental role in the response examined.

HOX-1 and COX-2 cytoprotective role during the oxidative challenge

In our previous study [6] we observed that C2 skeletal myoblasts viability was affected by H_2O_2 treatment only when high doses were used (at least 1 mM) decreasing to ~ 80% compared to control values (100%). This result, combined with HOX-1 and COX-2 observed up-regulation by H_2O_2, led us to probe into their potential contribution to C2 myoblasts tolerance under oxidative stress. Thus, using ZnPP, an established heme oxygenase activity inhibitor [29], we found C2 myoblasts survival rates to be further suppressed after treatment with 1 mM H_2O_2 in the presence of 5 μM ZnPP by ~ 20.5 ± 1.2% and by ~ 26.6 ± 2.2% at 10 μM ZnPP, respectively (Table I). ZnPP was not detected to have any toxic effect under normal conditions.

The potential cytoprotective function of COX-2 under oxidative stress was next assessed. In particular, the simultaneous presence of COX-2 selective inhibitor sc236 [30], along with 1 mM H_2O_2, was found to further suppress cell viability at both concentrations tested, which are routinely used in literature, by ~ 24.5 ± 2.2% at 5 μM and ~ 29.6 ± 3.2% at 10 μM, respectively (Table I). The inhibitor alone did not cause any toxic effect under normal conditions. In an effort to clarify the mechanism via which COX-2 exerts its beneficial role, we next assessed the levels of PGE_2, a marker of COX-2 activity. As shown in Figure 8, PGE_2 levels were considerably stimulated within 4 h of treatment with increasing concentrations of H_2O_2, peaking up at 1 mM of H_2O_2 (46.54 ± 2.56 pg/ml vs 14.55 ± 1.45 pg/ml in control), verifying COX-2 activation under the interventions studied. Suppressing COX-2 activity by pre-treatment with sc236 (at 5 and 10 μM) abrogated the observed effects. This finding implicates PGE_2 biosynthesis and release in the mechanism regulating COX-2 contribution to skeletal myoblasts exhibited tolerance, during an oxidative challenge.

Table I. Table presenting (%) cell viability assessment by MTT assay. C2 skeletal myoblasts were left untreated (Ctr) or treated with H_2O_2 (1 mM) in the presence or absence of either 5 μM or 10 μM of ZnPP or sc236 for 24 h. Values are means ± SE for at least four independent experiments.

Conditions	% Cell viability (M ± SE)
Ctr	100
5 μM ZnPP	91.2 ± 4.0
10 μM ZnPP	91.5 ± 4.5
1 mM H_2O_2	81.5 ± 1.5*
5 μM ZnPP + 1 mM H_2O_2	63.0 ± 1.0$^{\perp}$
10 μM ZnPP + 1 mM H_2O_2	58.0 ± 2.0$^{\perp}$
Ctr	100
5 μM sc236	99.0 ± 5.8
10 μM sc236	94.6 ± 6.50
1 mM H_2O_2	79.5 ± 6.5*
5 μM sc236 + 1 mM H_2O_2	60.0 ± 3.2$^{\perp}$
10 μM sc236 + 1 mM H_2O_2	56.0 ± 3.5$^{\perp}$

*$p < 0.01$ compared to control values and $^{\perp}$ $p < 0.001$ compared to identically treated cells in the absence of the inhibitor (two-tailed Student's t-test).

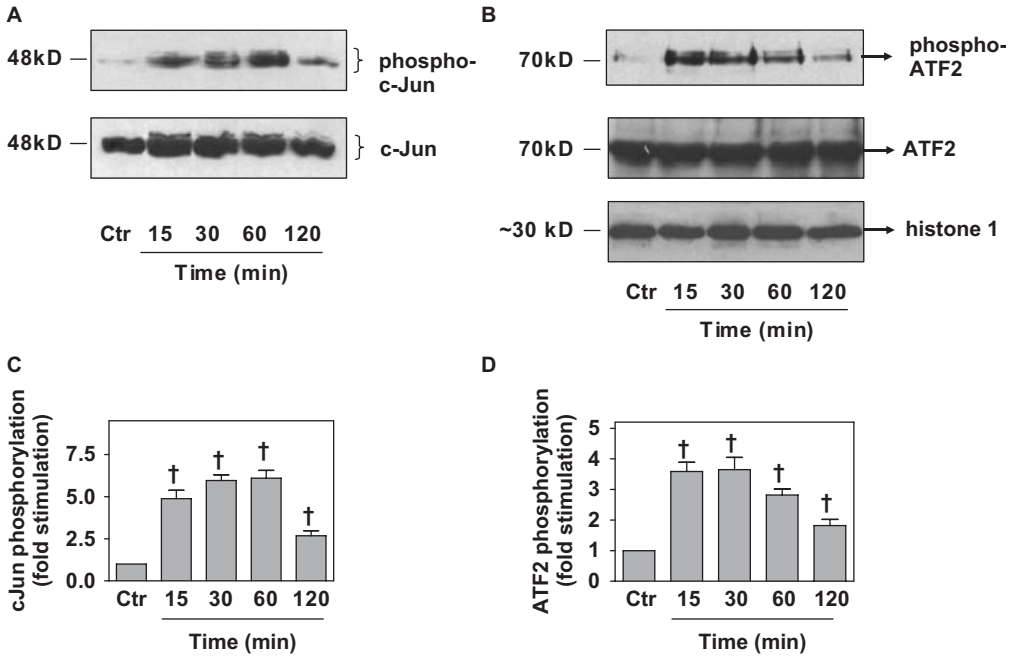

Figure 6. Time course of H_2O_2-induced c-Jun (A) and ATF2 (B) phosphorylation in C2 skeletal myoblasts. Cells were left untreated (Ctr) or incubated with 0.5 mM H_2O_2 for the times indicated. Nuclear extracts (30 µg) were subjected to SDS-PAGE and immunoblotted with an antibody for phosphorylated c-Jun (Ser63), ATF2 (Thr71) (A and B top panels, respectively) or against total levels of c-Jun (A, bottom panel), ATF2 (B, middle panel) and histone 1 (B, bottom panel). Respective protein band size is indicated on the left of the panels. Bands were quantified by laser scanning densitometry (C and D). Blots and results shown are representative of at least three independent experiments. Results are means ± SE for at least three independent experiments. $^{\dagger}p < 0.001$ compared to control values (one-way ANOVA with Tukey post-test).

Discussion

The multiple adverse conditions that cells face trigger responses which ultimately determine their fate. Redox equilibrium disturbances in particular, constitute a routine particularly in tissues characterized by a high rated oxidative metabolism (e.g. heart, brain, skeletal muscle fibres). Although reactive oxygen species (ROS) generated under a variety of physiological

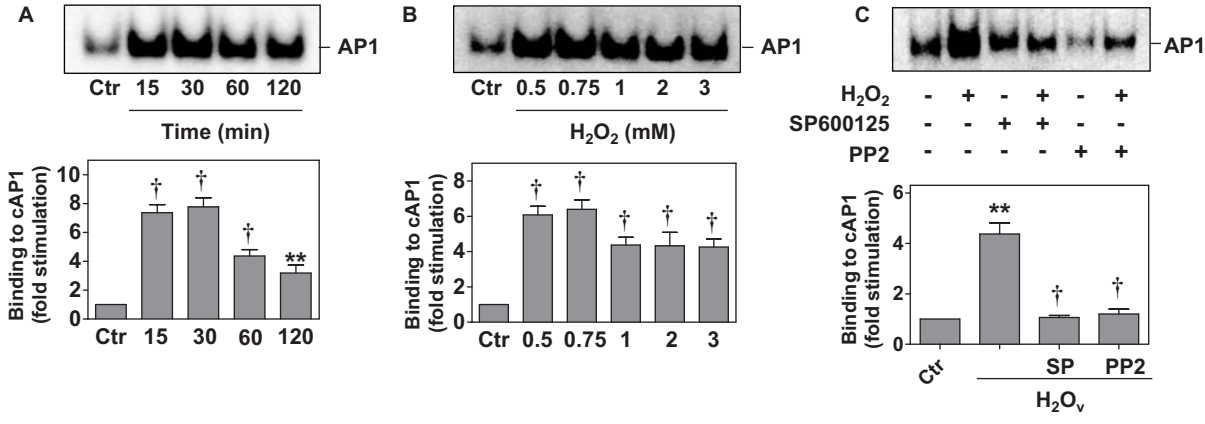

Figure 7. Transcription factor binding to a cAP-1 sequence is stimulated by H_2O_2. (A) C2 skeletal myoblasts were exposed to 0.5 mM H_2O_2 for the times indicated. Nuclear extracts were analysed by EMSA. (B): Dose-dependent pattern of AP-1 binding activity after exposure of cells to diverse H_2O_2 concentrations for 30 min. Cells were left untreated (Ctr) or incubated with H_2O_2. Representative autoradiographs are presented from at least three independent experiments with similar results. Graphs: Densitometric analysis of autoradiographs represented in the respective panels A and B. Results are means ± SE for at least three independent experiments. $^{**}p < 0.05$, $^{\dagger}p < 0.001$ compared to control values (one-way ANOVA with Tukey post-test). (C) JNKs and Src potentially contribute to H_2O_2-induced AP-1 binding activity. C2 skeletal myoblasts were left untreated (Ctr) or pre-incubated with 10 µM SP600125 (+SP) or 10 µM PP2 (+PP2) for 30 min and then exposed to 0.5 mM H_2O_2 for 30 min, in the absence or presence of the inhibitors. A representative autoradiograph is presented from at least three independent experiments with similar results. Results are means ± SE for at least three independent experiments. $^{\dagger}p < 0.001$ compared to identically treated cells in the absence of the respective inhibitor (two-tailed Student's *t*-test).

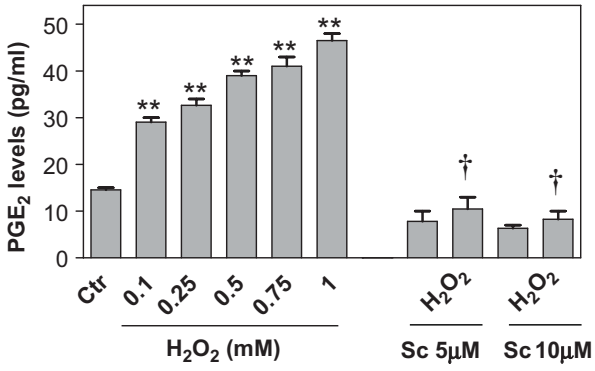

Figure 8. Dose-dependent H_2O_2-induced PGE_2 biosynthesis and the inhibitory effect of sc236. C2 skeletal myoblasts were left untreated (Ctr), exposed to increasing concentrations of H_2O_2 for 4 h or pre-incubated with 5 µM or 10 µM sc236 for 30 min and then exposed to 0.5 mM H_2O_2 for 4 h, in the presence of the inhibitor. The condition media were collected and PGE_2 levels were assessed using an EIA kit. Data are expressed as means ± SE for at least three independent experiments. $^{**}p < 0.05$ compared to control values (one-way ANOVA with Tukey post-test) and $^{\dagger}p < 0.001$ compared to identically treated cells in the absence of the inhibitor (two-tailed Student's *t*-test).

conditions have been reported to function as signalling molecules at low levels, their increase above a critical threshold leads to detrimental effects and has been implicated in the pathogenesis of several diseases [31,32]. Compared to other cell types, skeletal muscle cells are capable of adapting to intense redox imbalances, exhibiting a remarkable tolerance. This feature can be attributed to the cytoprotective antioxidative mechanisms activated under these conditions, eliciting their salutary effects via i.e. up-regulation of enzymatic or non-enzymatic effectors [8]. Despite the plethora of studies investigating ROS imbalances–stimulated injury or the triggered compensatory adaptations as muscle regeneration or growth, principally elicited by myoblasts, the molecular mechanisms involved remain elusive. To this end, we made an effort to delineate the signal transduction pathways coordinating the response of skeletal myoblasts to H_2O_2, along with the potentially beneficial physiological role of HOX-1 and COX-2, which have been previously reported to contribute to cytoprotection under adverse redox conditions in various experimental models [25,33].

As far as HOX-1 is concerned, mounting evidence has underlined its key role in physiology and disease, via the effects of heme degradation products. Among the three known HOX isoforms (HOX-1, -2 and -3) that have been identified in mammals, HOX-1 is highly inducible by oxidative stress, hypoxia and ultraviolet irradiation [12,34]. HOX-1 has emerged as a major survival protein, restoring and preserving homeostasis via its anti-apoptotic, anti-inflammatory and anti-oxidant activities [35]. Particularly in skeletal muscle, it has been shown to be induced during ischemia, exercise or in the case of certain muscular

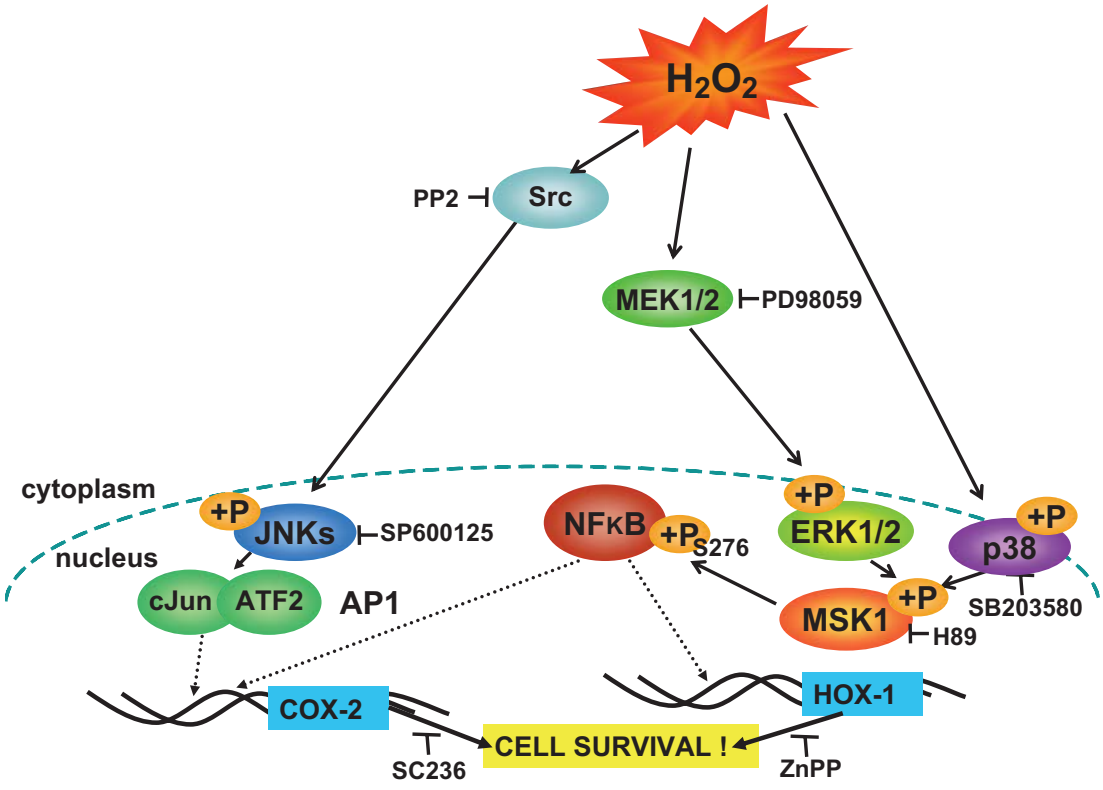

Figure 9. Schematic representation of a hypothetical model describing the signalling pathways involved in HOX-1 and COX-2 transcriptional regulation in response to H_2O_2 treatment, mediating C2 skeletal myoblast survival. → activation, —| inhibition.

diseases involving ROS [36,37]. Accordingly, in the present study, we have demonstrated HOX-1 expression to be stimulated with a rapid and prolonged profile after exposure to H_2O_2, (Figures 1 and 2, top), a finding that could indicate HOX-1 potential beneficial role under such adverse conditions.

As far as COX-2 pathway is concerned, it has been reported to play a fundamental role in the early stages of skeletal muscle regeneration after injury or disease [17]. Furthermore, Otis et al. [3] have denoted that COX-2 is crucial for stretch-induced primary myoblast proliferation via synthesis of prostaglandins: PGE_2 and PGF_{2a}. We therefore next investigated COX-2 potential contribution to C2 skeletal myoblasts response under oxidative stress. Indeed, we found COX-2 mRNA as well as protein levels to be significantly induced by H_2O_2 (Figures 1 and 2, middle), a result that correlates well with previous reports in rat mesangial cells [38] or keratinocytes [39].

Subsequently, we probed into the diverse signalling mechanisms involved in HOX-1 and COX-2 up-regulation under oxidative stress. Thus, while ERK1/2, p38-MAPK and MSK1 appear to participate in both HOX-1 and COX-2 response, the latter also constitutes a downstream target for JNKs and Src kinase (Figures 3 and 4). The potential cross-talk and interaction between these effectors appears to coordinate HOX-1 and COX-2 response during the oxidative challenge, ensuring exertion of their physiological role. ERK1/2 pathway has been previously reported to mediate HOX-1 gene expression [19,40,41], with various reports also marking p38-MAPK involvement in HOX-1 regulation under various conditions [42–44]. MSK1 has also been previously established to act as a mediator of HOX-1 induction in H9c2 cardiac myoblasts exposed to oxidative stress [18]. However, contradicting JNKs involvement in HOX-1 up-regulation by H_2O_2 in H9c2 cells or by ferric protoporphyrin and cobalt protoporphyrin in glioblastoma C6 cells [45], no involvement of JNKs was detected in the responses triggered in the present study. As far as COX-2 regulation is concerned, our findings are in line with several previous studies demonstrating ERK1/2, p38-MAPK, MSK1, JNKs and Src kinase involvement in COX-2 response to a plethora of stimuli in various cell types [16,46–49]. However, there are also reports marking no ERK1/2 or Src involvement in COX-2 regulation, i.e. after exposure of intestinal epithelial cells to collagen [50]. Evidently, our experimental data supports that the involvement of MAPKs in the regulation of both HOX-1 and COX-2 is cell type- and stimulus-specific.

In light of the results implicating MAPKs and MSK1 in the mechanisms regulating H_2O_2-induced HOX-1 and COX-2 responses, we next assessed their sub-cellular distribution, indicative of their role. Our results reveal that the nuclear compartment functions as a convergence locus for the accumulation of MAPKs (data not shown) and MSK1 activities (Figure 5A). This is in accordance with H_2O_2-induced activation of ERK1/2, JNKs and p38-MAPK in various cell types [21], as well as with the reported nuclear localization signal (NLS) in the C-terminal domain of MSK1 [51]. Another effector shown to be located in the nucleus (Figure 5B), previously observed to be transactivated in skeletal myoblasts exposed to oxidative stress by our group [6], is NF-κB. ERK1/2, p38-MAPK and MSK1 were found to mediate the phosphorylation of the nucleus localized p65 subunit of NF-κB at Ser276 (Figure 5B), denoting that the latter is another MAPK downstream substrate, potentially implicated in the observed responses. Indeed, several reports have marked NF-κB fundamental role in COX-2 [3,52] as well as HOX-1 regulation [53–55].

Given the active consensus sites for both NF-κB and AP1 sites in HOX-1 as well as COX-2 reported promoter regions [49,53], we next sought to determine the possible role of AP1, another redox-sensitive transcription factor, under these interventions. We initially examined the time profile of c-Jun and ATF2 phosphorylation (Figure 6) and observed that it correlated well with the time-dependent profile of AP1 DNA binding activity (Figure 7A). These results are indicative of AP1 potential participation in the signalling pathways triggered in the present study, in agreement with existing reports highlighting AP1 involvement in COX-2 regulation [52,56]. Furthermore, H_2O_2-induced AP1 DNA binding activity was demonstrated to be JNK- and Src-dependent, in accordance with a study by Harada et al. [57] reporting the Src kinase/JNKs/c-Jun/AP1 pathway to mediate arsenite-induced HOX-1 up-regulation in murine embryonic fibroblasts.

Taking into consideration the aforementioned results, one may deduce that the signalling pathways contributing to skeletal myoblasts tolerance under oxidative stress comprise of the following sequentially activated mediators: p38-MAPK and ERK1/2 → MSK1 → NF-κB → potentially regulating both HOX-1 and COX-2 and Src → JNKs→ AP1 regulating the COX-2 response.

Unlike the impressive body of evidence that has established HOX-1 as a cell survival mediator in diverse *in vitro* and *in vivo* models of oxidant-induced cellular and tissue injury [58], controversy surrounds the role of COX-2. Thus, although a pro-survival role of COX-2 has been shown in various experimental models as diverse as human lung, renal and cardiac cells [16,32,59–62], COX-2 activity has also been associated with acute ischemia-induced myocardial damage [63] and traumatic brain injury [64]. Therefore, we subsequently set out to assess the precise physiological role of these two effectors, in the experimental setting examined. Concomitant with the established notion of HOX-1 beneficial effects, hindering HOX-1

activity by using zinc protoporphyrin (ZnPP), resulted in further deterioration of C2 myoblasts survival rates after treatment with H_2O_2 (Table I). Accordingly, in the presence of sc236, which is known to inhibit COX-2 activity, C2 myoblasts survival was also further repressed after treatment with the oxidant (Table I). This result substantiates COX-2 salutary effects and establishes its contribution to the tolerance exhibited by skeletal myoblasts during an oxidative insult, comprising one of the principal findings of the present study. In an attempt to decipher the mechanism via which COX-2 exerts its observed beneficial role, we next assayed PGE_2 levels released in the culture medium of H_2O_2-treated cells, which are indicative of COX-2 activation and were found to be upregulated (Figure 8); in the presence of sc236, a profound reduction in PGE_2 levels was observed (Figure 8). This finding is in agreement with a study by Otis et al. [3] noting PGE_2 biosynthesis to be crucial for COX-2 contribution to stretch-induced primary myoblasts proliferation, as well as with the detected prostaglandin up-regulation by H_2O_2 [13].

Collectively, our results provide evidence regarding the molecular mechanisms contributing to skeletal myoblasts exquisite tolerance under oxidative stress. This novel data articulate the key salutary role of both HOX-1 and COX-2 and also decipher the signal transduction pathways involved in their regulation (summarized in Figure 9). Depending on their temporal, spatial and quantitative activation profiles and via their interaction, these mediators orchestrate the observed cellular responses, ensuring preservation of homeostasis. Gaining insight in these molecular mechanisms is of extreme importance and could contribute to the development of new therapeutic interventions and strategies 'against' skeletal muscle disorders triggered by oxidative imbalances.

Declaration of interest: This work was funded by grants of the Special Research Account of the University of Athens. The authors report no conflicts of interest. The authors alone are responsible for the content and writing of the paper.

References

[1] Thannickal VJ, Fanburg BL. Reactive oxygen species in cell signaling. Am J Physiol Lung Cell Mol Physiol 2000;279: 1005–1028.

[2] Bhatnagar S, Kumar A. Therapeutic targeting of signaling pathways in muscular dystrophy. J Mol Med 2010;88:155–166.

[3] Otis JS, Burkholder TJ, Pavlath GK. Stretch-induced myoblast proliferation is dependent on the COX2 pathway. Exp Cell Res 2005;310:417–425.

[4] Hawke TJ, Garry DJ. Myogenic satellite cells: physiology to molecular biology. J Appl Physiol 2001;91:534–551.

[5] Yaffe D, Saxel O. Serial passaging and differentiation of myogenic cells isolated from dystrophic mouse muscle. Nature 1977;270:725–727.

[6] Kefaloyianni E, Gaitanaki C, Beis I. ERK1/2 and p38-MAPK signalling pathways, through MSK1, are involved in NF-kappaB transactivation during oxidative stress in skeletal myoblasts. Cell Signal 2006;18:2238–2251.

[7] Ardanaz N, Pagano PJ. Hydrogen peroxide as a paracrine vascular mediator: regulation and signaling leading to dysfunction. Exp Biol Med 2006;231:237–251.

[8] West JD, Marnett LJ. Endogenous reactive intermediates as modulators of cell signaling and cell death. Chem Res Toxicol 2006;19:173–194.

[9] Niess AM, Sommer M, Schneider M, Angres C, Tschositch K, Golly IC, Battenfeld N, Northoff H, Biesalski HK, Dickhuth HH, Fehrenbach E. Physical exercise-induced expression of inducible nitric oxide synthase and heme oxygenase-1 in human leukocytes: effects of RRR-alpha-tocopherol supplementation. Antioxid Redox Signal 2000;2:113–126.

[10] Maines MD. The heme oxygenase system: update 2005. Antioxid Redox Signal 2005;7:1761–1766.

[11] Applegate LA, Luscher P, Tyrell RM. Induction of heme oxygenase: a general response to oxidant stress in cultured mammalian cells. Cancer Res 1991;51:974–978.

[12] Keyse SM, Tyrell RM. Heme oxygenase is the major 32-kDa stress protein induced in human skin fibroblasts by UVA radiation, hydrogen peroxide, and sodium arsenite. Proc Natl Acad Sci USA 1989;86:99–103.

[13] Karayalcin SS, Sturbaum CW, Washmann JT, Cha JH, Powell DW. Hydrogen peroxide stimulates rat colonic prostaglandin production and alters electrolyte transport. J Clin Inv 1990;86:60–68.

[14] Williams CS, Mann M, Dubois RN. The role of cyclooxygenases in inflammation, cancer, and development. Oncogene 1999;18:7908–7916.

[15] Yang CM, Chien CS, Wang CC, Hsiao LD. Interleukin-1beta-induced cyclooxygenase-2 expression is mediated through activation of p42/44 and p38 MAPKS, and NF-kappaB pathways in canine tracheal smooth muscle cells. Cell Signal 2002;14:899–911.

[16] Yang T, Huang Y, Heasley L, Berl T, Schnermann JB, Briggs JP. MAPK mediation of hypertonicity-stimulated cyclooxygenase-2 expression in renal medullary collecting duct cells. J Biol Chem 2000;275:23281–23286.

[17] Bondesen BA, Mills ST, Kegley KM, Pavlath GK. The COX-2 pathway is essential during early stages of skeletal muscle regeneration. Am J Physiol Cell Physiol 2004;287:C475–C483.

[18] Aggeli IK, Gaitanaki C, Beis I. Involvement of JNKs and p38-MAPK/MSK1 pathways in H2O2-induced upregulation of heme oxygenase-1 mRNA in H9c2 cells. Cell Signal 2006;18:1801–1812.

[19] Zhang X, Bedard EL, Potter R, Zhong R, Alam J, Choi A, Lee P. Mitogen-activated protein kinases regulate HO-1 gene transcription after ischemia-reperfusion lung injury. Am J Physiol Lung Cell Mol Physiol 2002;283:L815–L829.

[20] Kyriakis JM, Avruch J. Sounding the alarm: protein kinase cascades activated by stress and inflammation. J Biol Chem 1996;271:24313–24316.

[21] Martindale JL, Holbrook NJ. Cellular response to oxidative stress: signaling for suicide and survival. J Cell Physiol 2002;192:1–15.

[22] Zhou LZ, Johnson AP, Rando TA. NF kappa B and AP-1 mediate transcriptional responses to oxidative stress in skeletal muscle cells. Free Radic Biol Med 2001;31:1405–1416.

[23] Vermeulen L, De Wilde G, Damme PV, Vanden Berghe W, Haegeman G. Transcriptional activation of the NF-kappaB p65 subunit by mitogen- and stress-activated protein kinase-1 (MSK1). EMBO J 2003;22:1313–1324.

[24] Mosmann T. Rapid colorimetric assay for cellular growth and survival: application to proliferation and cytotoxicity assays. J Immunol Methods 1983;65:55–63.

[25] Araujo JA, Meng L, Tward A, Hancock WW, Zhai Y, Lee A, Ishikawa K, Iyer S, Buelow R, Busuttil RW, Shih DM, Lusis

AJ, Kupiec JW. Systemic rather than local heme oxygenase-1 overexpression improves cardiac allograft outcomes in a new transgenic mouse. J Immunol 2003;171:1572–1580.
[26] Buschmann T, Yin Z, Bhoumik A, Ronai Z. Amino-terminal-derived JNK fragment alters expression and activity of c-Jun, ATF2, and p53 and increases H2O2-induced cell death. J Biol Chem 2000;275:16590–16596.
[27] Livingstone C, Patel G, Jones N. ATF-2 contains a phosphorylation-dependent transcriptional activation domain. EMBO J 1995;14:1785–1797.
[28] Herdegen T, Leah JD. Inducible and constitutive transcription factors in the mammalian nervous system: control of gene expression by Jun, Fos and Krox, and CREB/ATF proteins. Brain Res Rev 1998;28:370–490.
[29] Fang J, Sawa T, Akaike T, Greish K, Maeda H. Enhancement of chemotherapeutic response of tumor cells by a heme oxygenase inhibitor, pegylated zinc protoporphyrin. Int J Cancer 2004;109:1–8.
[30] Ko SC, Chapple KS, Hawcroft G, Coletta PL, Markham AF, Hull ML. Paracrine cyclooxygenase-2-mediated signalling by macrophages promotes tumorigenic progression of intestinal epithelial cells. Oncogene 2002;21:7175–7186.
[31] Vercherat C, Chung TK, Yalcin S, Gulbagci N, Gopinadhan S, Ghaffari S, Taneja R. Stra13 regulates oxidative stress mediated skeletal muscle degeneration. Hum Mol Genet 2009;18:4304–4316.
[32] Murphy ME, Keherer JP. Oxidative stress and muscular dystrophy. Chem Biol Interact 1989;69:101–173.
[33] Eliqini S, Arenaz I, Dourado PM, da Luz PL, Chagas AC. Cyclooxygenase-2 mediates hydrogen peroxide-induced wound repair in human endothelial cells. Free Radic Biol Med 2009;46:1428–1436.
[34] Motterlini R, Foresti R, Bassi R, Calabrese V, Clark JE, Green CJ. Endothelial heme oxygenase-1 induction by hypoxia. Modulation by inducible nitric-oxide synthase and S-nitrosothiols. J Biol Chem 2000;275:13613–13620.
[35] Bach FH. Heme oxygenase-1: a therapeutic amplification funnel. FASEB J 2005;19:1216–1219.
[36] Hellsten Y, Nielsen JJ, Lykkesfeldt J, Bruhn M, Silveira L, Pilegaard H, Bangsbo J. Antioxidant supplementation enhances the exercise-induced increase in mitochondrial uncoupling protein 3 and endothelial nitric oxide synthase mRNA content in human skeletal muscle. Free Radic Biol Med 2007;43:353–361.
[37] Pachori AS, Melo LG, Hart ML, Noiseux N, Zhang L, Morello F, Solomon SD, Stahl GL, Pratt RE, Dzau VJ. Hypoxia-regulated therapeutic gene as a preemptive treatment strategy against ischemia/reperfusion tissue injury. Proc Natl Acad Sci USA 2004;101:12282–12287.
[38] Feng L, Xia Y, Garcia GE, Hwang D, Wilson CB. Involvement of reactive oxygen intermediates in cyclooxygenase-2 expression induced by interleukin-1, tumor necrosis factor-alpha, and lipopolysaccharide. J Clin Invest 1995;95:1669–1675.
[39] Ashida M, Bito T, Budiyanto A, Ichihashi M, Ueda M. Involvement of EGF receptor activation in the induction of cyclooxygenase-2 in HaCaT keratinocytes after UVB. Exp Dermatol 2003;12:445–452.
[40] Chen K, Maines MD. Nitric oxide induces heme oxygenase-1 via mitogen-activated protein kinases ERK and p38. Cell Mol Biol 2000;46:609–617.
[41] Song HJ, Shin CY, Oh TY, Min YS, Park ES, Sohn UD. Eupatilin with heme oxygenase-1-inducing ability protects cultured feline esophageal epithelial cells from cell damage caused by indomethacin. Biol Pharm Bull 2009;32:589–596.
[42] Wijayanti N, Kietzmann T, Immenschuh S. Heme oxygenase-1 gene activation by the NAD(P)H oxidase inhibitor 4-(2-aminoethyl) benzenesulfonyl fluoride via a protein kinase B, p38-dependent signaling pathway in monocytes. J Biol Chem 2005;280:21820–21829.
[43] Kacimi R, Chentoufi J, Honbo N, Long CS, Karliner J. Hypoxia differentially regulates stress proteins in cultured cardiomyocytes: role of the p38 stress-activated kinase signaling cascade, and relation to cytoprotection. Cardiovasc Res 2000;46:139–150.
[44] Hsu CL, Wu YL, Tang GJ, Lee TS, Kou YR. Ginkgo biloba extract confers protection from cigarette smoke extract-induced apoptosis in human lung endothelial cells: role of heme oxygenase 1. Pulm Pharmacol Ther 2009;22:286–296.
[45] Chow JM, Huang GC, Lin HY, Shen SC, Yang LY, Chen YC. Cytotoxic effects of metal protoporphyrins in glioblastoma cells: roles of albumin, reactive oxygen species, and heme oxygenase-1. Toxicol Lett 2008;177:97–107.
[46] Hunot S, Vila M, Teismann P, Davis RJ, Hirsch EC, Przedborski S, Rakic P, Flavell RA. JNK-mediated induction of cyclooxygenase 2 is required for neurodegeneration in a mouse model of Parkinson's disease. Proc Natl Acad Sci USA 2004;101:665–670.
[47] Jang BC. Induction of COX-2 in human airway cells by manganese: role of PI3K/PKB, p38 MAPK, PKCs, Src, and glutathione depletion. Toxicol In Vitro 2009;23:120–126.
[48] Sun H, Xu B, Inoue H, Chen QM. P38 MAPK mediates COX-2 gene expression by corticosterone in cardiomyocytes. Cell Signal 2008;20:1952–1959.
[49] Chen JJ, Huang WC, Chen CC. Transcriptional regulation of cyclooxygenase-2 in response to proteasome inhibitors involves reactive oxygen species-mediated signaling pathway and recruitment of CCAAT/enhancer-binding protein delta and CREB-binding protein. Mol Biol Cell 2005;16:5579–5591.
[50] Broom OJ, Massoumi R, Sjolander A. Alpha2beta1 integrin signalling enhances cyclooxygenase-2 expression in intestinal epithelial cells. J Cell Physiol 2006;209:950–958.
[51] Deak M, Clifton AD, Lucocq LM, Alessi DR. Mitogen- and stress-activated protein kinase-1 (MSK1) is directly activated by MAPK and SAPK2/p38, and may mediate activation of CREB. EMBO J 1998;17:4426–4441.
[52] Kim SH, Oh JM, No JH, Bang YJ, Juhn YS, Song YS. Involvement of NF-kappaB and AP-1 in COX-2 upregulation by human papillomavirus 16 E5 oncoprotein. Carcinogenesis 2009;30:753–757.
[53] Arruda MA, Rossi AG, de Freitas MS, Barja-Fidalgo C, Graça-Souza AV. Heme inhibits human neutrophil apoptosis: involvement of phosphoinositide 3-kinase, MAPK, and NF-kappaB. J Immunol 2004;173:2023–2030.
[54] Lin CC, Chiang LL, Lin CH, Shih CH, Liao YT, Hsu MJ, Chen BC. Transforming growth factor-beta1 stimulates heme oxygenase-1 expression via the PI3K/Akt and NF-kappaB pathways in human lung epithelial cells. Eur J Pharmacol 2007;60:101–109.
[55] Wijayanti N, Huber S, Samoylenko A, Kietzmann T, Immenschuh S. Role of NF-kappaB and p38 MAP kinase signaling pathways in the lipopolysaccharide-dependent activation of heme oxygenase-1 gene expression. Antioxid Redox Signal 2004;6:802–810.
[56] Zhang D, Li J, Song L, Ouyang W, Gao J, Huang C. A JNK1/AP-1-dependent, COX-2 induction is implicated in 12-O-tetradecanoylphorbol-13-acetate-induced cell transformation through regulating cell cycle progression. Mol Cancer Res 2008;6:165–174.
[57] Harada H, Sugimoto R, Watanabe A, Taketani S, Okada K, Warabi E, Siow R, Itoh K, Yamamoto M, Ishii T. Differential roles for Nrf2 and AP-1 in upregulation of HO-1 expression by arsenite in murine embryonic fibroblasts. Free Radic Res 2008;42:297–304.
[58] Shibahara S. Regulation of heme protein synthesis. Dayton, OH: Alpha Med Press; 1994.
[59] Joo JH, Jetten AM. NF-kappaB-dependent transcriptional activation in lung carcinoma cells by farnesol involves p65/RelA(Ser276) phosphorylation via the MEK-MSK1 signaling pathway. J Biol Chem 2008;283:16391–16399.

[60] Huhn R, Heinen A, Weber NC, Hieber S, Hollmann MW, Schlack MW, Preckel B. Helium-induced late preconditioning in the rat heart *in vivo*. Br J Anaesth 2009;102:614–619.
[61] Adderley SR, Fitzgerald DJ. Oxidative damage of cardiomyocytes is limited by extracellular regulated kinase 1/2-mediated induction of cyclooxygenase-2. J Biol Chem 1999;274:5038–5046.
[62] Camitta MG, Gabel SA, Chulada P, Bradbury JA, Langenbach R, Zeldin DC. Cyclooxygenase-1 and -2 knockout mice demonstrate increased cardiac ischemia/reperfusion injury but are protected by acute preconditioning. Circulation 2001;104:2453–2458.
[63] Carnieto A, Dourado PM, Da Luz PL, Chagas AC. Selective cyclooxygenase-2 inhibition protects against myocardial damage in experimental acute ischemia. Clinics 2009;64:245–252.
[64] Strauss KI, Barbe MF, Marshall RM, Raghupathi R, Mehta S, Narayan RK. Prolonged cyclooxygenase-2 induction in neurons and glia following traumatic brain injury in the rat. J Neurotrauma 2000;17:695–711.

This paper was first published online on Early Online on 7 April 2010.